RSC Advances

PAPER

View Article Online
View Journal | View Issue

Cite this: *RSC Adv.*, 2023, **13**, 23947

A computational study on the coordination modes and electron absorption spectra of the complexes U(IV) with *N*,*N*,*N*′,*N*′-tetramethyl-diglycolamide and anions†

Yating Yang, Youshi Lan, Qian Liu, Liyang Zhu, Xuan Hao, Jin Zhou, Suliang Yang* and Guoxin Tian*

Lipophilic *N*,*N*,*N*′,*N*′-tetraalkyl-diglycolamides (TRDGAs) are promising extractants for actinides separation in spent nuclear fuel reprocessing. Usually, in the extracted complexes of actinide and lanthanide ions of various oxidation states, the metal ions are completely surrounded by 2 or 3 TRDGA molecules, and the counter anions do not directly coordinate with them. In contrast, the extracted complexes of U(IV) from different media presenting different absorption spectra indicate that the anions (Cl^- and NO_3^-) are directly involved in the coordination with U(IV) in the first inner sphere. Based on this exceptional observation in solvent extraction, taking the coordination of U(IV) with *N*,*N*,*N*′,*N*′-tetramethyl-diglycolamide (TMDGA, the smallest analogue of TRDGA) as the research object, we mimic the behaviours of counterions (Cl^- and NO_3^-) and the water molecule during coordination of TMDGA with U(IV), especially combining with the simulation of the absorption spectra. We demonstrate that during the complexing of TMDGA to U(IV), the counterion Cl^- will occupy one coordination number in the inner coordination sphere, and NO_3^- will occupy two by bidentate type; however, the ubiquitous water cannot squeeze in the inner coordination sphere. In addition, the coordination of Cl^- and NO_3^- is proved to favour the extraction with the lower binding energy. Moreover, the simulation of absorption spectra is in good agreement with the observation from experiments, further verifying the aforementioned conclusion. This work in some way will provide guidance to improve the computation methods in research of actinides by mimicking the absorption spectra of actinide ions in different complexes.

Received 23rd June 2023
Accepted 3rd August 2023

DOI: 10.1039/d3ra04206e

rsc.li/rsc-advances

1. Introduction

Nuclear energy has been successfully developed to generate civil electricity for over 70 years. Currently, most nuclear power plants are mainly using enriched uranium (about 4–5%) oxide as fuel, and the common fuel cycling period is about 12 to18 months. For each cycle, the used fuel needs to be discharged out of and new fuel needs to be refilled into the reactors. The used fuel consists of about 96% fissile and fertile material, small amounts of minor actinides, and 3% fission products. The 96% fissile and fertile material includes unused uranium (95%) and by-produced plutonium by uranium capturing neutrons (1%), which are useful and can be recovered to manufacture new fuel. The minor actinides including Np, Am, and Cm are in relatively small amounts, but they are the major contributors to the long-term radioactive toxicity in the used fuel. In recent decades, in order to develop sustainable nuclear energy by more efficiently utilizing the limited uranium resource and to reduce the volume of high-level waste, partitioning–transmutation (P–T) strategy has been developed and related research has been conducted to some extended degree.[2,3] By P–T strategy, besides uranium and plutonium are recovered from used fuel to make new fuel, minor actinides are also separated from fission products, especially lanthanides, and further transmuted into short-lived or stable nuclides in dedicated reactors or accelerator-driven systems.

To match the varying needs of P–T strategy for the separations of actinides, specific reagents and processes have to be developed and practically tested. Due to the radiotoxicity of actinides, it is very cost to conduct the associated experiments. Hence, computation methods become more attractive in the related research of actinides. However, there is a dilemma for utilizing computation methods. In one hand, reliable computation methods may provide alternative approaches to eliminate some difficult experiments and to reduce the cost of handling

Department of Radiochemistry, China Institute of Atomic Energy, Beijing 102413, China. E-mail: ysl79@ciae.ac.cn; gtian@ciae.ac.cn

† Electronic supplementary information (ESI) available. See DOI: https://doi.org/10.1039/d3ra04206e

actinides in common research laboratories. In the other hand, the computation methods suitable for accurately solving the problems in investigating actinide materials have not been well developed. Because of the complexed electronic structure, significant f-electron correlation effects, and relativistic effects of actinides, accurate computations and simulations are still a challenge in actinide chemistry. Therefore, developing suitable approaches is essential for enhancing the application of computation technique in researches of actinide instead of experimental methods involving radioactive materials.

Besides, spectroscopy is a powerful tool to study the coordination chemistry of actinides. When absorbing photons at a certain energy (the visible to near infrared region), the f-electrons of actinides might transfer from low-energy orbitals to higher ones, that is, f–f transition. By analysing the molecular spectra and clarifying the transition behaviour between electronic states, one can figure out the bonding properties of f-orbitals in actinide complexes. The vibrational spectroscopy (such as infrared spectroscopy, Raman spectroscopy) and electronic spectroscopy (such as absorption spectroscopy and fluorescence spectroscopy) have been frequently-used to study the coordination chemistry of actinides.[4–7]

With the development of quantum chemistry, intensive researches on the coordination and spectrochemistry of actinides by means of theoretical simulation have sprung up with respect of compatible with experimental observation.[8–20] Potentially, density functional theory (DFT) is able to accurately predict the static electronic properties of actinide complexes and to explain their behaviour in separation processes and migration in environment, but when considering the absorption spectra, only DFT even time-dependent DFT method is invalid for the consideration of multireference characteristics, which should be supplemented by the post Hartree–Fock method. To sum up, with well optimized geometry, by combining frequency analysis with excitation simulation, the vibrational spectra and electronic spectra of the complexes might be mimicked, and by combining the simulation of electronic structure with thermodynamic characteristics, the observed experimental phenomena might be explained.

In this work, we chose the coordination of U(IV) with water-soluble ligand *N*,*N*,*N*′,*N*′-tetramethyl-diglycolamide (TMDGA)[21,22] in aqueous solution as the research object in comparison with the extraction of U(IV) using in *N*,*N*′-dimethyl-*N*,*N*′-dioctyl-diglycolamide (DMDODGA) in solvent extraction. Basically, the solvent extraction is the most frequently-used method for the separation of lanthanides from actinides.[23–25] Since the 5f orbitals in actinides have a higher spatial distribution than the 4f orbitals in lanthanides, the formation of covalent bond in the former becomes easier.[26] Therefore, compared with Ln^{3+}, the An^{3+} is much softer to complex with softer elements. The chosen water-soluble ligands TMDGA shows excellent coordination ability with actinides, with three oxygen atoms strongly coordinating with the inner metal atom. Considering the environment of the ordinary solution, counterions widely exist, who will influence the separation of actinides to some extent. Usually, counterions in the outer sphere are regarded as 'spectator ions', which in general are mainly used for charge balancing or space filling but have little effect on the chemical reactions.[27] However, Liu *et al.* showed that, TMDGA can complex with U(IV) with the ratio of U(IV) : TMDGA of 1 : 1, 1 : 2 and 1 : 3 in 1 M HCl and 1 M HNO_3. Moreover, the different spectral performance in HCl and HNO_3 and the diffusion reflectance spectrum is attributed to the influence of counterions, who are hypothesized to appear in the inner coordination sphere.[1] This finding contradicts the previous experimental results that the NO_3^- counterion is demonstrated to only appear in the outer coordination sphere and not directly bond with Pu(IV) in the 1 : 3 complex of TMGDA-Pu(IV) based on the vis-NIR spectra and crystal structures.[28] Therefore, whether the counterions will exist in the first coordination sphere and how they will influence the extraction needs a deep analysis.

Based on this, comprehensive static and electronic properties, molecular dynamics and spectra analysis has been performed. The behaviours of counterions (Cl^- and NO_3^-) and the water molecule during coordination of TMDGA with U(IV) are analysed by optimizing the geometries, mimicking the binding energy and comparing the simulated spectra with the experimental observation. The calculation demonstrates that with three TMDGA molecules bonded to U(IV), water–U(IV)–TMDGA is not energy-favourable, which means that the water will not appear in the inner coordination sphere; on the contrary, Cl^- and NO_3^- can reduce the binding energy of the 1 : 3 U(IV)–TMDGA complex when appears in the first coordination sphere. Meanwhile, the simulation of electronic structures and absorption spectra imply that the U(IV)–TMDGA complex can only afford one coordination site for Cl^-, while for NO_3^-, the two-sited bidentate coordination is energetically more favourable. The research clarifies the complexation behaviour of counterions in the solvent extraction process from the perspective of spectroscopy simulation and confirms that counterions can appear in the inner coordination sphere and affect the complexing of TMDGA with U(IV). The work is significant for understanding the complexation properties of actinides, as well as paving the way for the development of spectral simulation for actinides.

2. Computational details

Geometric optimization and electronic structure characterizations were carried out with Gaussian16 software package[29] at B3LYP level[30–33] in gas phase. Amongst, Standard pople's 6-31G* basis set were used during initial static electronic structural calculations for the light C, H, O, N and Cl elements,[34] and the Stuttgart relativistic effective core potential (RECPs) was selected for the heavier U atom, with ECP60MWB basis set.[35,36] The accurate single-point energy calculations was switched to TPSSH level[37] with def2TZVP[38]/ECP60MWB[35,36] basis set for the light and heavier elements, in aqueous environment. It is worth noting that the crystal structure of 1 : 3 U(IV)–TMDGA is directly provided by the experiment, thus its geometric optimization was carried out with all atoms fixed expect for the H atoms, whereas other structures was optimized without constraints. The convergence criteria kept the default values.

Ab initio molecular dynamics (AIMD) were accomplished in CP2K/QUICKSTEP package based on the Gaussian and plane waves method (GPW),[39,40] with Perdew–Burke–Ernzerhof (PBE) exchange-correlation functional.[41] The Goedecker, Teter and Hutter (GTH) pseudopotentials and corresponding MOLOPT basis sets were employed for the light C, H, O, N, and Cl atoms,[42] and the norm-conserving pseudopotentials and basis sets developed by Lu *et al.* for uranium.[43] Cutoff energy was set as 600 Ry. Here, a 20 Å-sided cube was applied, with more than 200 water molecules added randomly to mimic the real solution environment. Counterions (Cl^-, NO_3^- or ClO_4^-) were added to neutralize system charge. Periodicity was considered in all three directions.

Absorption spectra were performed with ORCA software package (version 4.2),[44] with the complete active space self-consistent field (CASSCF)[45] combining with n-electron valence state perturbation theory (NEVPT2)[46–49] method. The scalar relativistic effect was described with the second order Douglas–Kroll–Hess (DKH2) method,[50] combining with spin–orbit coupling (SOC) effect. Amongst, U was treated with SARC-DKH-TZVP basis set,[51] and the others were with DKH-TZVP.[52,53] Based on the previous report,[46] seven 5f orbitals and five 6d orbitals were selected as the active space to accurately mimic the spectra, with two of the seven 5f orbitals occupied and all the other ten orbitals empty, including five 5f orbitals and five 6d orbitals. Since the 5f orbitals are somewhat be affected by 6d orbitals but have neglectable influence from 7s orbitals, meanwhile, other bonding and anti-bonding orbitals have even higher energy levels than 7s, which will result in the transition beyond the detected spectral region, the selection of active space is necessary and enough. Besides, both singlet and triplet were taken into consideration, with 50 excited states set for each. Mulliken charge analysis and orbital analysis was performed by using the Multiwfn 3.7 software.[54]

3. Results and discussion

3.1 Geometric optimization and electronic structures characterization

According to experimental conditions, a molecular of water, Cl^- and NO_3^- ions are inserted to the original 1 : 3 U(IV)–TMDGA in the first coordination sphere, shown in Fig. 1, detailed xyz formats are listed in ESI.† The structure of bare U(IV)–TMDGA is directly provided by the experiment.[1] It should be noted that, the optimization is performed with C, O and U atoms fixed in bare U(IV)–TMDGA system to maintain the experimental condition and release all atoms in other self-built structures. For H_2O–U(IV)–TMDGA complex, the molecule of water is pushed away from the inner coordination sphere during the optimization, due to the uncompetitive inter-molecular interaction and strong steric-hindrance effect. In Cl–U(IV)–TMDGA complex, only one Cl^- can be inserted. When forcefully inserting two Cl^-s, one of the three TMDGAs will be got rid of with only one O atom coordinated with U(IV). As for the NO_3^-, since its spatial scale is large, we only consider a single NO_3^-. There are three equivalent O atoms in NO_3^-, so monodentate and bidentate type should all be taken into consideration.[55] *Ab initio* molecular dynamic simulations were carried out to further verify the results, where the water molecular will escape from the first coordinate sphere after 1 ps, as well as two Cl^-s, while the other counterions will maintain within the inner sphere of U(IV), as shown in Fig. S1 in ESI.† It is worth noting that, after 1 ps, the bidentate type of NO_3^- shows the characteristic of monodentate, it is because of the concentration of NO_3^- is too low to reprint the real solvent condition.

Table 1 summarizes the averaged interatomic distance between the 9 coordinated O atoms with U(IV), and that between U(IV) and the inserted Cl^-/NO_3^-. Since the water cannot be inserted into U(IV)–TMDGA complex during optimization, we will not discuss it in this part. Amongst, the 2.40 Å in pure U(IV)–TMDGA is determined by experiments.[1] When a Cl^- is inserted, the TMDGA ligands are pushed away from the centered U atom, with the averaged bond length at 2.51 Å. After optimization, the mono-type shows a smaller U–O bond length even than Cl^-, while bi-type shows a little bit longer bond length due to its requirement of space. Actually, the 0.05 Å difference may not have huge influence on their stability. In a word, the inserted counterions will extend the filling space of the whole complex, with the TMDGA pushed away from U(IV). But anyway, the calculated bond lengths around the covalent radius clarifies that the counterions can coordinate to U(IV) in the inner coordination sphere.

Further, we calculate the Mulliken charge distribution[56] for the above four systems, Table 2. In general, the O atoms in TMDGA and counterions are regarded as an electron donor, and U(IV) as an electron acceptor. On the whole, in pure TMGDA–U(IV) complex, the Mulliken charge localized at U is 2.784. When inserted with Cl^- and NO_3^-, the value becomes lower,

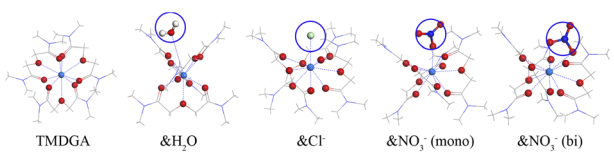

Fig. 1 Geometric schematic diagram of U(IV)–TMDGA complexes with and without water and counterions Cl^-, NO_3^- after optimization. It's worth noting that, the water will be pushed away during optimization, which will not appear in the first inner coordination sphere. The red, blue and green ball represents the oxygen, uranium and chloride atom separately.

Table 1 Averaged simulated interatomic distance between the centered U and electron-donor atoms in U(IV)–TMDGA complexes. U–O means the averaged interatomic distance between the 9 coordinated O atoms in TMDGA with U(IV), and the U–Cl/O(NO_3^-) means the distance between U and the connected Cl or O atom in counterions. The C, O and U atoms are fixed in the pure U(IV)–TMDGA during optimization to illustrate the experimental geometry,[1] whereas all atoms are released in the &Cl^-/&NO_3^- system

(Unit: Å)	&Cl^-	&NO_3^- (mono)	&NO_3^- (bi)	TMDGA (exp.)[1]
U–O	2.51	2.50	2.56	2.40
U–Cl/O(NO_3^-)	2.65	2.28	2.49	

Table 2 Mulliken charge analysis for U(IV)–TMDGA complexes. Amongst, TMDGA represents pure U(IV)–TMDGA complex, and the others are U(IV)–TMDGA complexes with counterions Cl^- and NO_3^-. *U* represents the calculated charge around U atom, $Cl^-/O(NO_3^-)$ means charge around Cl^- or around the jointed O atom in NO_3^-, and Cl^-/NO_3^- is the charge in the whole Cl^-/NO_3^- counterion

	&Cl^-	&NO_3^- (mono)	&NO_3^- (bi)	TMDGA
U	2.466	2.771	2.522	2.784
$Cl^-/O(NO_3^-)$	−0.394	−0.490	−0.373	
Cl^-/NO_3^-	−0.394	−0.169	−0.124	

indicating more electrons are accepted by U(IV), especially in the &Cl^- complex. For the part of counterions, the Mulliken charge left in Cl^- is −0.394, and that in NO_3^- is −0.490 and −0.373 separately for the mono- and bi-dentate type which means Cl^- transfers more electron to U(IV) than mono-typed NO_3^- but less than bi-typed NO_3^-. The last row represents the Mulliken charge for the whole liganded counterions. The naked ions should be −1, thus the difference is due to the flow of electrons from ligand to the centered U. Due to the different contribution of TMDGAs, the negative charge left in Cl^- is larger than that in NO_3^-, reverse of the conclusion from the positive charge in U, who is more suitable to describe the metal–ligand interaction. Obviously, the flow of electrons demonstrates that the direct coordination with counterions and U(IV) in the inner coordination sphere is possible.

Besides, we depict all seven 5f-dominant molecular orbitals in &Cl^-, &NO_3^- (mono) and &NO_3^- (bi) complex, shown in Fig. 2(a), from SOMO-1 (SOMO, Single Occupied Molecular Orbital) to SOMO + 5. Amongst, all seven 5f-dominant orbitals are shown around U element, with slightly p orbital appears around Cl^- and NO_3^- fragment, which is circled by red, blue and green curve. The same iso-surface value was used. The delocalization around p and f orbitals in &Cl^- system indicates a stronger covalent interaction between U(IV) and Cl^-. Whereas, the monodentate &NO_3^- shows a more obvious delocalization than bidentate type, due to its shorter bond length than bidentate type, Table 1. The values shown in Fig. 2(b) clarify the statement, where the composition of f orbitals become lower and p become higher in Cl^- complex. The results agree well with our previous analysis.

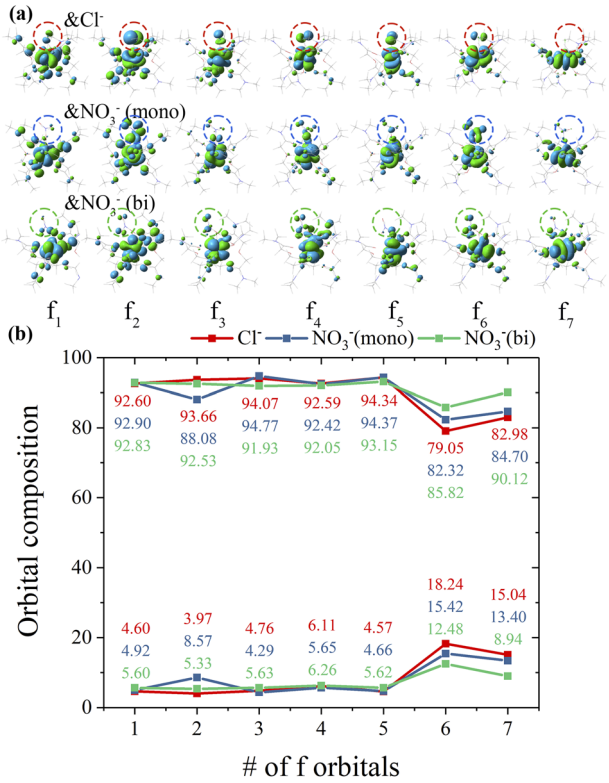

Fig. 2 Orbital analysis in U(IV)–TMDGA coordinated with counterions Cl^- and NO_3^-. (a) shows f-type molecular orbitals in U(IV)–TMDGA complexes. Here, the 5f-dominant orbitals are around the U element, accompanied by some p orbitals from Cl^- and NO_3^-. The dotted circles represent the Cl^- and two types of NO_3^-. (b) shows the accurate orbital compositions in each system and each orbital from SOMO-1 to SOMO + 5.

3.2 Binding energy

Furthermore, we calculate the binding energy (BE) for each U(IV)–TMDGA complex according to the following formula, listed in Table 3. The chosen initial structure is $U(TMDGA)_3^{4+}$.

$$U(TMDGA)_3^{4+} + \text{counterion } (Cl^-/NO_3^-) \rightarrow U(TMDGA)_3(\text{counterion})^{3+} \quad (1)$$

$$U(TMDGA)_3^{4+} + H_2O \rightarrow U(TMDGA)_3(H_2O)^{4+} \quad (2)$$

It is worth noting that, here we forcefully fix the position of O in H_2O molecular to mimic its binding energy, otherwise the H_2O molecule will escape from the first coordination sphere. Besides, only one molecule of counterion or water is taken into consideration due to the space limitation. We can directly point out that, with a positive binding energy, the coordination with an extra water is energy-unfavourable. Again, we confirm that no water molecular will appear in the inner coordination sphere. Whereas, &Cl^- and &NO_3^- show the negative binding energy, which means they are easier to coordinate with U(IV) in the presence of 3 TMDGAs. Amongst, Cl^- is the easiest counterion to coordinate, the next is bidentate NO_3^-, whose binding energy is 3.36 kJ mol^{-1} lower than the monodentate type. From the energetic standpoint, Cl^- and NO_3^- can all exist in the first coordination sphere, meanwhile, they both can lower the binding energy of the U(IV)–TMDGA complex, which in this perspective, the counterions can promote the extraction of U(IV) by TMDGA.

3.3 Absorption spectra

By electronic and energy analysis, counterions are verified to appear in the first inner coordinate sphere in 1 : 3 U(IV)–TMDGA complex. Meanwhile, geometric optimization, molecular dynamics and binding energy simulation demonstrates its behaviour. Further, under the guidance of experiments and our recent research findings,[1,46] we take use of absorption spectra as

Table 3 The summarized binding energy (BE) for U(IV)–TMDGA with the inserted counterions and the water molecular. Amongst, only one Cl^-, NO_3^- and water is considered, with two types of NO_3^- ligand (monodentate and bidentate). The O atom in H_2O is fixed during optimization in &H_2O system, merely to obtain the binding energy, otherwise it will escape from the first coordination sphere. $E_{complexes}$ is the total energy of each U(IV)–TMDGA complexe, $E_{U(TMDGA)_3^{4+}}$ is the energy of pure U(IV)–TMDGA complex, and $E_{counterion/H_2O}$ is the energy of a single counterion or water molecular

	$E_{complexes}$ (Hartree)	$E_{U(TMDGA)_3^{4+}}$(Hartree)	$E_{counterion/H_2O}$(Hartree)	BE (Hartree)	BE (kJ mol^{-1})
&H_2O	−2501.40	−2424.95	−76.48	0.032	85.24
&Cl^-	−2885.21	−2424.95	−460.22	−0.048	−126.90
&NO_3^- (mono)	−2705.48	−2424.95	−280.52	−0.011	−28.22
&NO_3^- (bi)	−2705.48	−2424.95	−280.52	−0.012	−31.58

a tool to deeply investigate the underlying mechanism for counterions coordinated with U(IV)–TMDGA complex. It is worth mentioning that, Lan *et al.* summarized 11 distinguished computation methods to mimic the absorption spectrum of hydrated tetravalent uranium and pointed out that, the complete active space self-consistent field (CASSCF) integrating n-electron valence state perturbation theory (NEVPT2), combining with Douglas–Kroll–Hess (DKH) method and spin–orbit coupling (SOC) effect can accurately describe the characteristics of the excited states of actinides and the electron transitions between them.[46] Thus, making use of the approach, we performed the simulation of the absorption spectra of the targeted U(IV)–TMDGA complexes, both to verify the accuracy of the aforementioned algorithm and to clarify the behaviour of counterions during extraction of U(IV) by TMDGA.

As shown in Fig. 3(a) is the absorption spectrum of non-ligand U(IV)–TMDGA complex, noting that 3 perchlorate ions (ClO_4^-) are symmetrically introduced to mimic the real condition, and the geometric illustration is shown in Fig. S2 in ESI.† (b)–(d) are complexes with counterions Cl^- and NO_3^- coordinating in the first inner coordination sphere. (e) is grabbed from the experimental result,[1] with primary peaks a_0 to k_0 at 670.0, 659.3, 653.0, 625.8, 551.3, 541.0, 491.5, 477.3, 465.8, 432.5 and 418.0 nm. (c) and (d) are separately for monodentate and bidentate NO_3^- complex, with one and two oxygens coordinating with U(IV). By comparing the simulation and experiment, the bidentate-type complex shows a more similar characteristic to the experiment especially for the rough intensity and distribution of each peak, while, the monodentate-type complex shows characteristics far away from the experiment. A few details that differ from the experiment are due to the simplification of simulation models, since in the real solution the concentration of counterions is largely excess.

From perspective of absorption spectra, we speculate that the bidentate-type coordination of NO_3^- is the dominant existence form in U(IV)–TMDGA, even if they both have similar binding energy and electronic structure. Then, by fixing the wavenumber of the most intuitive major peak f in Fig. 3(d) the same as the f_0 in Fig. 3(e), and shift the spectrum, the all 4 spectra become comparable with the experiment, the translation distance of wavenumber is 3139 cm^{-1}. Actually, the absolute position of each peak cannot be simulated exactly, but compared with the non-ligand U(IV)–TMDGA complex, the complexes with counterions all show a slightly blue shift, which is in agreement with the experiment.[1]

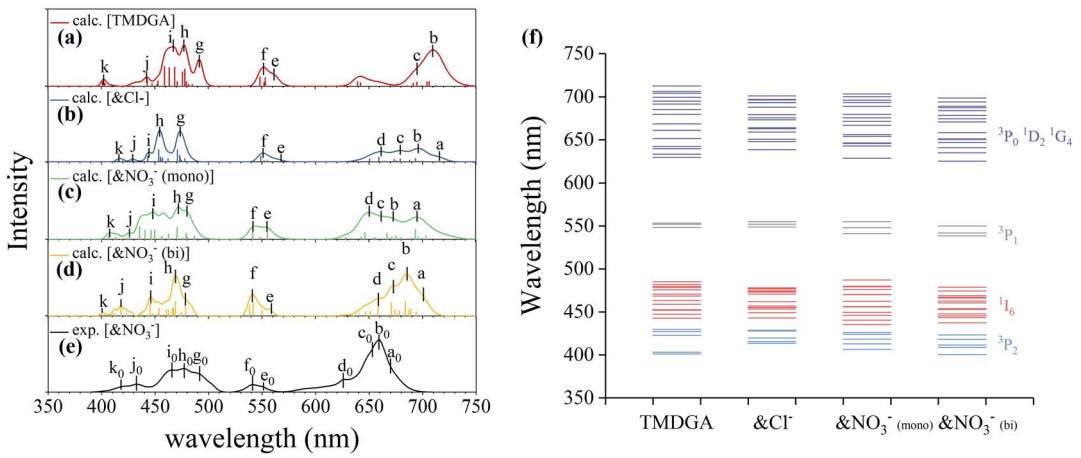

Fig. 3 The absorption spectra of non-ligand (a) U(IV)–TMDGA complex and (b)–(d) complexes with counterions Cl^-, NO_3^- coordinating in the first inner coordination sphere. (e) is extracted from experimental results.[1] Amongst, (c) is the monodentate- and (d) is the bidentate-typed coordination. The colored vertical lines in (a)–(d) are energy levels of each orbital. (f) is the related energy levels of each orbital and the identification of excited states in the experimental range of 350 to 750 nm. Besides, primary peaks are selected and labeled from a/a_0 to k/k_0, the exact wavelengths are listed in Table S1 in ESI.†

The electronic configuration of U(IV) is $5f^2$ with 2 electrons left in seven 5f orbitals, which leads to 7 spectral terms and further be separated into 13 spectral branches, corresponding to 91 microscopic states (90 excited electronic states and a ground states) in U(IV) complexes, listed in Table S1 in ESI.† The 13 spectral branches are, $^3H_4$, $^3F_2$, $^3H_5$, $^3F_3$, $^3F_4$, $^3H_6$, $^3P_0$, $^1D_2$, $^1G_4$, $^3P_1$, $^1I_6$, $^3P_2$ and $^1S_0$. Amongst, a/a_0 to k/k_0 in Fig. 3(a)–(e) belongs to $^3P_0$, $^1D_2$, $^1G_4$, $^3P_1$, $^1I_6$ and $^3P_2$, which are not forbidden and can be detected in the experimental range of 350 to 750 nm, as shown in Fig. 3(f), and details are listed in Table S1 in ESI.† Since there are only two electrons left in U(IV), the values in the top left corner only show 1 and 3, meaning the singlet and triplet state. The first spectral branch, $^3H_4$, is the ground state of U(IV), which has a degeneracy of 9, with the character of coupling both singlet and triplet state. The contribution percentage of singlet/triplet state in $^3H_4$ of pure U(IV)–TMDGA, &Cl^-, &NO_3^-(mono) and &NO_3^-(bi) complexes is 9.3%/90.7%, 8.6%/91.4%, 8.4%/91.6%, and 8.6%/91.4%. Obviously, the ground states of these complexes are dominant by triple state, but with unneglectable 10% singlet character. In reality, both ground and excited states of these complexes show multi-configuration character. Thus, the consideration of multi-configurational character is necessary. The last spectral branch $^1S_0$ corrosponds to the highest electron exitation, with wavelength at around 250 to 350 nm. Peaks lower than $^1S_0$ are attributed to the 5f → 6d transition, which were not depicted here. Peaks above 350 nm corresponds to the weak 5f → 5f transition with low absorption. Actually, the 5f → 5f transition is supposed to be forbbiden, which is relieved because of the viriation of orbitals and structures bringing by the coordination with ligand, but the intensity is weak. While, the mentioned 5f → 6d transition is not forbidden, leading to a much stronger excitation intensity at the lower wavelength. In reality, there are several hiden states between $^1S_0$ and $^3P_2$, origining from the transtion between 5f and 6d orbitals, but no states in the pure $U(H_2O)_9^{4+}$ complex.[46] This is due to the coordination of U(IV) with ligands, who lifts these transitions than $^1S_0$. The simulations agree well with the previous paper,[57–59] verifying the accuracy of the computation method for the absorption spectra.

4. Conclusions

In summary, the research uncovers the behaviour of counterions (Cl^- and NO_3^-) and the water molecule during extraction of U(IV) by TRDGA in the first inner coordination sphere. The geometric optimization, energetic analysis and molecular dynamics show that only one Cl^- can be inserted into the first coordination sphere of TMDGA–U(IV), and there is no more space to afford a second Cl^-. As for the NO_3^-, there will be two types of coordination forms, the mono- and bi-dentate. The lower formation energy indicates the bidentate type an energy-favourable type, meanwhile, by mimicking the absorption spectra and comparing with experiments, the bidentate type is further proved to be the dominant. Water cannot be accepted into the inner coordination sphere due to its weaker complexing capability. Our effort of introducing the photoelectronic spectra to analyse the species formed in solvent extraction is significant for deeply understanding the complexation chemistry of actinides. Moreover, the fairly accurate simulation of the absorption spectra verifies the precision of the group-developed algorithm, which afford guidance for further exploration of computation method for actinides.

Conflicts of interest

There are no conflicts to declare.

Notes and references

1 Q. Liu, J. Zhou, L. Zhu, D. Li, Y. Zhang, S. Yang and G. Tian, The complexation of U(IV) ion with N, N, N′, N′-Tetraalkyl-Diglycolamide in aqueous solutions and extraction systems of varying anions, *Inorg. Chem. Commun.*, 2022, **143**, 109730.
2 E.-M. Gonzalez-Romero, Impact of partitioning and transmutation on the high level waste management, *Nucl. Eng. Des.*, 2011, **241**(9), 3436–3444.
3 M. Salvatores and G. Palmiotti, Radioactive waste partitioning and transmutation within advanced fuel cycles: Achievements and challenges, *Prog. Part. Nucl. Phys.c*, 2011, **66**(1), 144–166.
4 K. O. Kvashnina and S. M. Butorin, High-energy resolution X-ray spectroscopy at actinide $M_{4,5}$ and ligand K edges: what we know, what we want to know, and what we can know, *Chem. Commun.*, 2022, **58**(3), 327–342.
5 M. A. Denecke, Actinide speciation using X-ray absorption fine structure spectroscopy, *Coord. Chem. Rev.*, 2006, **250**(7–8), 730–754.
6 S. M. Butorin, Advanced x-ray spectroscopy of actinide trichlorides, *J. Chem. Phys.*, 2021, **155**(16), 164103.
7 B. A. Maynard, K. S. Lynn, R. E. Sykora and A. E. Gorden, Emission, Raman spectroscopy, and structural characterization of actinide tetracyanometallates, *Inorg. Chem.*, 2013, **52**(9), 4880–4889.
8 S.-X. Hu, J. Qin, P. Zhang, M.-B. Shuai and P. Zhang, Theoretical insight into coordination chemistry of Am (VI) and Am (V) with phenanthroline ligand: implications for high oxidation state based minor actinide separation, *Inorg. Chem.*, 2020, **59**(9), 6338–6350.
9 Y. Gao, A. Jennifer G., E. Varathan and G. Schreckenbach, Understanding the Coordination Chemistry of Am^{III}/Cm^{III} in the DOTA Cavity: Insights from Energetics and Electronic Structure Theory, *Inorg. Chem.*, 2023, **7**(62), 3229–3237.
10 M. G. Ferrier, E. R. Batista, J. M. Berg, E. R. Birnbaum, J. N. Cross, J. W. Engle, H. S. La Pierre, S. A. Kozimor, J. S. Lezama Pacheco and B. W. Stein, Spectroscopic and computational investigation of actinium coordination chemistry, *Nat. Commun.*, 2016, **7**(1), 12312.
11 Z. Wang, N. Pu, Y. Tian, C. Xu, F. Wang, Y. Liu, L. Zhang, J. Chen and S. Ding, Highly selective separation of actinides from lanthanides by dithiophosphinic acids: an in-depth investigation on extraction, complexation, and DFT calculations, *Inorg. Chem.*, 2018, **58**(9), 5457–5467.

12 B. E. Klamm, C. J. Windorff, C. Celis-Barros, M. L. Marsh, D. S. Meeker and T. E. Albrecht-Schmitt, Experimental and theoretical comparison of transition-metal and actinide tetravalent Schiff base coordination complexes, *Inorg. Chem.*, 2018, **57**(24), 15389–15398.

13 J. Su, K. Zhang, W. E. Schwarz and J. Li, Uranyl-glycine-water complexes in solution: Comprehensive computational modeling of coordination geometries, stabilization energies, and luminescence properties, *Inorg. Chem.*, 2011, **50**(6), 2082–2093.

14 J. Su, Y.-L. Wang, F. Wei, W. E. Schwarz and J. Li, Theoretical study of the luminescent states and electronic spectra of UO_2Cl_2 in an argon matrix, *J. Chem. Theory Comput.*, 2011, **7**(10), 3293–3303.

15 P. D. Dau, J. Su, H.-T. Liu, J.-B. Liu, D.-L. Huang, J. Li and L.-S. Wang, Observation and investigation of the uranyl tetrafluoride dianion ($UO_2F_4^{2-}$) and its solvation complexes with water and acetonitrile, *Chem. Sci.*, 2012, **3**(4), 1137–1146.

16 J. Su, Z. Wang, D. Pan and J. Li, Excited states and luminescent properties of UO_2F_2 and its solvated complexes in aqueous solution, *Inorg. Chem.*, 2014, **53**(14), 7340–7350.

17 J. Su, E. R. Batista, K. S. Boland, S. E. Bone, J. A. Bradley, S. K. Cary, D. L. Clark, S. D. Conradson, A. S. Ditter and N. Kaltsoyannis, Energy-degeneracy-driven covalency in actinide bonding, *J. Am. Chem. Soc.*, 2018, **140**(51), 17977–17984.

18 J. Su, C. J. Windorff, E. R. Batista, W. J. Evans, A. J. Gaunt, M. T. Janicke, S. A. Kozimor, B. L. Scott, D. H. Woen and P. Yang, Identification of the formal +2 oxidation state of neptunium: synthesis and structural characterization of $\{Np^{II}[C_5H_3(SiMe_3)_2]_3\}^{1-}$, *J. Am. Chem. Soc.*, 2018, **140**(24), 7425–7428.

19 C. A. Goodwin, J. Su, L. M. Stevens, F. D. White, N. H. Anderson, J. D. Auxier, T. E. Albrecht-Schönzart, E. R. Batista, S. F. Briscoe and J. N. Cross, Isolation and characterization of a californium metallocene, *Nature*, 2021, **599**(7885), 421–424.

20 J.-J. Yang, Z. Zhao and J. Su, Theoretical Study of the Excited States and Luminescent Properties of $(H_2O)_n$ UO_2Cl_2 (n= 1-3), *Inorg. Chem.*, 2023, **62**(5), 1978–1987.

21 F. Kou, S. Yang, H. Qian, L. Zhang, C. M. Beavers, S. J. Teat and G. Tian, A fluorescence study on the complexation of Sm(III), Eu(III) and Tb(III) with tetraalkyldiglycolamides (TRDGA) in aqueous solution, in solid state, and in solvent extraction, *Dalton Trans.*, 2016, **45**(46), 18484–18493.

22 S. Pahan, A. Boda and S. M. Ali, Density functional theoretical analysis of structure, bonding, interaction and thermodynamic selectivity of hexavalent uranium (UO_2^{2+}) and tetravalent plutonium (Pu^{4+}) ion complexes of tetramethyl diglycolamide (TMDGA), *Theor. Chem. Acc.*, 2015, **134**, 1–16.

23 G. Modolo, A. Wilden, A. Geist, D. Magnusson and R. Malmbeck, A review of the demonstration of innovative solvent extraction processes for the recovery of trivalent minor actinides from PUREX raffinate, *Radiochim. Acta*, 2012, **100**(8–9), 715–725.

24 L. Fuks and M. Majdan, Features of solvent extraction of lanthanides and actinides, *Miner. Process. Extr. Metall. Rev.*, 2000, **21**(1–5), 25–48.

25 R. Wietzke, M. Mazzanti, J.-M. Latour, J. Pécaut, P.-Y. Cordier and C. Madic, Lanthanide(III) complexes of tripodal N-donor ligands: structural models for the species involved in solvent extraction of actinides (III), *Inorg. Chem.*, 1998, **37**(26), 6690–6697.

26 G. R. Choppin, Covalency in f-element bonds, *J. Alloys Compd.*, 2002, **344**(1–2), 55–59.

27 M. Moliner, F. Rey and A. Corma, Towards the rational design of efficient organic structure-directing agents for zeolite synthesis, *Angew. Chem., Int. Ed.*, 2013, **52**(52), 13880–13889.

28 S. D. Reilly, A. J. Gaunt, B. L. Scott, G. Modolo, M. Iqbal, W. Verboom and M. J. Sarsfield, Plutonium (IV) complexation by diglycolamide ligands-Coordination chemistry insight into TODGA-based actinide separations, *Chem. Commun.*, 2012, **48**(78), 9732–9734.

29 M. J. Frisch, G. W. Trucks, H. B. Schlegel, G. E. Scuseria, M. A. Robb, J. R. Cheeseman, G. Scalmani, V. Barone, G. A. Petersson, H. Nakatsuji, X. Li, M. Caricato, A. V. Marenich, J. Bloino, B. G. Janesko, R. Gomperts, B. Mennucci, H. P. Hratchian, J. V. Ortiz, A. F. Izmaylov, J. L. Sonnenberg, D. Williams-Young, F. Ding, F. Lipparini, F. Egidi, J. Goings, B. Peng, A. Petrone, T. Henderson, D. Ranasinghe, V. G. Zakrzewski, J. Gao, N. Rega, G. Zheng, W. Liang, M. Hada, M. Ehara, K. Toyota, R. Fukuda, J. Hasegawa, M. Ishida, T. Nakajima, Y. Honda, O. Kitao, H. Nakai, T. Vreven, K. Throssell, J. A. Montgomery Jr, J. E. Peralta, F. Ogliaro, M. J. Bearpark, J. J. Heyd, E. N. Brothers, K. N. Kudin, V. N. Staroverov, T. A. Keith, R. Kobayashi, J. Normand, K. Raghavachari, A. P. Rendell, J. C. Burant, S. S. Iyengar, J. Tomasi, M. Cossi, J. M. Millam, M. Klene, C. Adamo, R. Cammi, J. W. Ochterski, R. L. Martin, K. Morokuma, O. Farkas, J. B. Foresman and D. J. Fox, Wallingford, CT, 2016.

30 A. D. Becke, A new mixing of Hartree-Fock and local density-functional theories, *J. Chem. Phys.*, 1993, **98**(2), 1372–1377.

31 C. Lee, W. Yang and R. G. Parr, Development of the Colle-Salvetti correlation-energy formula into a functional of the electron density, *Phys. Rev. B*, 1988, **37**(2), 785.

32 S. H. Vosko, L. Wilk and M. Nusair, Accurate spin-dependent electron liquid correlation energies for local spin density calculations: a critical analysis, *Can. J. Phys.*, 1980, **58**(8), 1200–1211.

33 P. J. Stephens, F. J. Devlin, C. F. Chabalowski and M. J. Frisch, Ab initio calculation of vibrational absorption and circular dichroism spectra using density functional force fields, *J. Phys. Chem.*, 1994, **98**(45), 11623–11627.

34 M. M. Francl, W. J. Pietro, W. J. Hehre, J. S. Binkley, M. S. Gordon, D. J. DeFrees and J. A. Pople, Self-consistent molecular orbital methods. XXIII. A polarization-type basis

set for second-row elements, *J. Chem. Phys.*, 1982, **77**(7), 3654–3665.

35 X. Cao, M. Dolg and H. Stoll, Valence basis sets for relativistic energy-consistent small-core actinide pseudopotentials, *J. Chem. Phys.*, 2003, **118**(2), 487–496.

36 X. Cao and M. Dolg, Segmented contraction scheme for small-core actinide pseudopotential basis sets, *J. Mol. Struct.: THEOCHEM*, 2004, **673**(1–3), 203–209.

37 L. E. Aebersold and A. K. Wilson, Considering Density Functional Approaches for Actinide Species: The An66 Molecule Set, *J. Phys. Chem. A*, 2021, **125**(32), 7029–7037.

38 F. Weigend and R. Ahlrichs, Balanced basis sets of split valence, triple zeta valence and quadruple zeta valence quality for H to Rn: Design and assessment of accuracy, *Phys. Chem. Chem. Phys.*, 2005, **7**(18), 3297–3305.

39 J. Hutter, M. Iannuzzi, F. Schiffmann and J. VandeVondele, cp2k: atomistic simulations of condensed matter systems, *Wiley Interdiscip. Rev.: Comput. Mol. Sci.*, 2014, **4**(1), 15–25.

40 J. VandeVondele, M. Krack, F. Mohamed, M. Parrinello, T. Chassaing and J. Hutter, Quickstep: Fast and accurate density functional calculations using a mixed Gaussian and plane waves approach, *Comput. Phys. Commun.*, 2005, **167**(2), 103–128.

41 G. Lippert, J. Hutter and M. Parrinello, A hybrid Gaussian and plane wave density functional scheme, *Mol. Phys.*, 1997, **92**(3), 477–488.

42 S. Goedecker, M. Teter and J. Hutter, Separable dual-space Gaussian pseudopotentials, *Phys. Rev. B*, 1996, **54**(3), 1703.

43 J.-B. Lu, D. C. Cantu, C.-Q. Xu, M.-T. Nguyen, H.-S. Hu, V.-A. Glezakou, R. Rousseau and J. Li, Norm-conserving pseudopotentials and basis sets to explore actinide chemistry in complex environments, *J. Chem. Theory Comput.*, 2021, **17**(6), 3360–3371.

44 F. Neese, The ORCA program system, *Wiley Interdiscip. Rev.: Comput. Mol. Sci.*, 2012, **2**(1), 73–78.

45 B. O. Roos, P. R. Taylor and P. E. Sigbahn, A complete active space SCF method (CASSCF) using a density matrix formulated super-CI approach, *Chem. Phys.*, 1980, **48**(2), 157–173.

46 L. Youshi, Y. Suliang, L. Qian, Y. Yating, Z. Liyang and T. Guoxin, Relativistic Quantum Chemical Studies on Absorption Spectrum of Tetravalent Uranium Hydrate, *Energy Sci. Technol.*, 2023, **57**, 1–10.

47 C. Angeli, R. Cimiraglia, S. Evangelisti, T. Leininger and J.-P. Malrieu, Introduction of n-electron valence states for multireference perturbation theory, *J. Chem. Phys.*, 2001, **114**(23), 10252–10264.

48 C. Angeli, R. Cimiraglia and J.-P. Malrieu, n-electron valence state perturbation theory: A spinless formulation and an efficient implementation of the strongly contracted and of the partially contracted variants, *J. Chem. Phys.*, 2002, **117**(20), 9138–9153.

49 C. Angeli, M. Pastore and R. Cimiraglia, New perspectives in multireference perturbation theory: the n-electron valence state approach, *Theor. Chem. Acc.*, 2007, **117**, 743–754.

50 A. Wolf, M. Reiher and B. A. Hess, The generalized douglas-kroll transformation, *J. Chem. Phys.*, 2002, **117**(20), 9215–9226.

51 D. A. Pantazis and F. Neese, All-electron scalar relativistic basis sets for the actinides, *J. Chem. Theory Comput.*, 2011, **7**(3), 677–684.

52 D. A. Pantazis, X.-Y. Chen, C. R. Landis and F. Neese, All-electron scalar relativistic basis sets for third-row transition metal atoms, *J. Chem. Theory Comput.*, 2008, **4**(6), 908–919.

53 A. Schäfer, C. Huber and R. Ahlrichs, Fully optimized contracted Gaussian basis sets of triple zeta valence quality for atoms Li to Kr, *J. Chem. Phys.*, 1994, **100**(8), 5829–5835.

54 T. Lu and F. Chen, Multiwfn: A multifunctional wavefunction analyzer, *J. Comput. Chem.*, 2012, **33**(5), 580–592.

55 M. Mihaylov, V. Zdravkova, E. Ivanova, H. Aleksandrov, P. S. Petkov, G. Vayssilov and K. Hadjiivanov, Infrared spectra of surface nitrates: Revision of the current opinions based on the case study of ceria, *J. Catal.*, 2021, **394**, 245–258.

56 R. S. Mulliken, Electronic population analysis on LCAO-MO molecular wave functions. I, *J. Chem. Phys.*, 1955, **23**(10), 1833–1840.

57 I. Richman, P. Kisliuk and E. Wong, Absorption Spectrum of U^{4+} in Zircon ($ZrSiO_4$), *Phys. Rev.*, 1967, **155**(2), 262.

58 M. F. Reid and F. S. Richardson, Parameterization of electric-dipole intensities in the vibronic spectra of rare-earth complexes, *Mol. Phys.*, 1984, **51**(5), 1077–1094.

59 R. Satten, C. Schreiber and E. Wong, Vibronic intensity parametrization for the UCl^{2-}_6 complex in crystals, *J. Chem. Phys.*, 1983, **78**(1), 79–87.